Journal of Fluids and Structures 27 (2011) 659–667

Contents lists available at ScienceDirect

Journal of Fluids and Structures

journal homepage: www.elsevier.com/locate/jfs

Football curves

Guillaume Dupeux [a,b], Caroline Cohen [a,b], Anne Le Goff [a,b], David Quéré [a,b], Christophe Clanet [a,b,*]

[a] LadHyX, UMR7646 du CNRS, Ecole Polytechnique, 91128 Palaiseau, France
[b] PMMH, UMR7636 du CNRS, ESPCI, 10 rue Vauquelin, 75005 Paris, France

A R T I C L E I N F O

Article history:
Received 3 December 2010
Accepted 30 March 2011
Available online 8 May 2011

Keywords:
Football
Ball trajectories
Spinning ball
Physics of sport

A B S T R A C T

Straight lines, zigzag, parabolas (possibly truncated), circles and spirals are the main curves which can be observed in football (in the European sense, soccer elsewhere). They are, respectively, associated to heavy kick, knuckleball, lob and banana kicks. We discuss their physical origin and determine their respective domain of existence.

1. Introduction

The earliest traces of ball games date back 3400 years (Hill et al., 1998). These games are part of man evolution (Blanchard, 2005) and one finds them over the different continents (Fig. 1): Tsu Chu in China, Kemari in Japan (Guttmann and Thompson, 2001), Episkiros in Greece (Craig, 1961; Miller, 2006) and Pok a tok in South America (Hosler et al., 1988).

In its present form, the rules of football originate from October 26, 1863 (Murray, 1998): on that day, the London schools and sports club sent representatives to the Freemason's Tavern, where the Football Association was formed. Rugby supporters left this association six years later when the modern rules forbidding the use of hands in the game were definitely adopted.

Studies on the physics of soccer mainly involve mechanics and statistics. The latter started in 1968 with the seminal work of Charles Reep[1] and Brooke Benjamin on the *Skill and Chance in Association Football* (Reep and Benjamin, 1968). This first study was then extended by the authors to other sports (Reep et al., 1971). Later, statistical physics tools were used to approach other questions such as the distribution of goals (Malacarne and Mendes, 2000; Greenhough et al., 2002), the statistics of ball touches (Mendes et al., 2007) or the final ranking in different championships (Ribeiro et al., 2010).

On the mechanical side, the studies can be split into two main categories: respectively dedicated to the ball trajectory (Mehta, 1985; Carre et al., 2002; Dupeux et al., 2010) and to the impact on the ball (Bull Andersen et al., 1999; Asai et al., 2002; Haddadin et al., 2009; Ishii et al., 2009).

In this paper, we discuss the different ball trajectories which can be observed in football and their associated physics.

2. Phase diagram

Three main forces are at play to determine the ball trajectory: the gravitational force F_G, the forces associated to the surrounding fluid, that is, the drag F_D and the lift F_L. We propose to discuss football curves in the phase diagram ($D_r = F_D/F_G$, $S_P = F_L/F_D$)

* Corresponding author at: LadHyX, UMR7646 du CNRS, Ecole Polytechnique, 91128 Palaiseau, France.
E-mail address: clanet@ladhyx.polytechnique.fr (C. Clanet).

[1] About the major influence of Charles Reep on soccer strategy, see Larson (2001).

0889-9746/$ - see front matter
doi:10.1016/j.jfluidstructs.2011.03.022

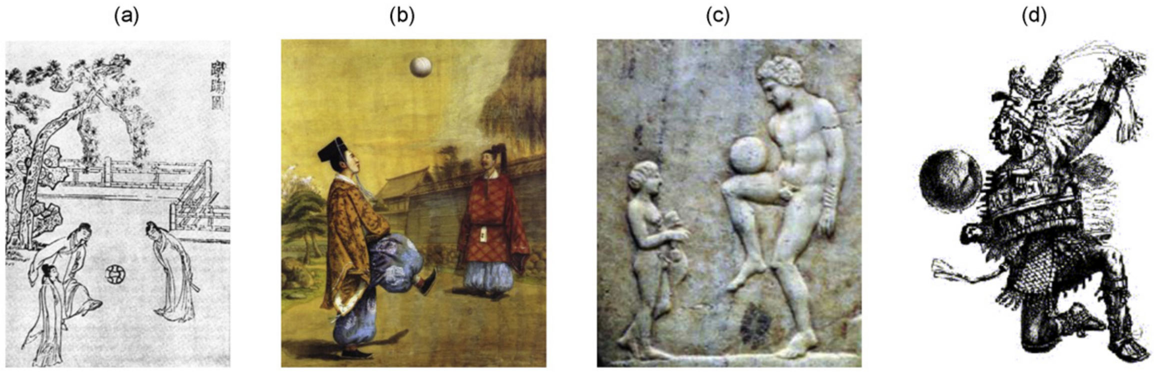

Fig. 1. Ancient ball games: (a) Chinese Tsu Chu, (b) Japanese Kemari, (c) Greek Episkiros and (d) Maya Pok a Tok. (Sources: (a) http://www.footballnetwork.org, (b) National Football Museum, Preston, UK, (c) National Archaeological Museum, Athens, (d) http://www.greatdreams.com).

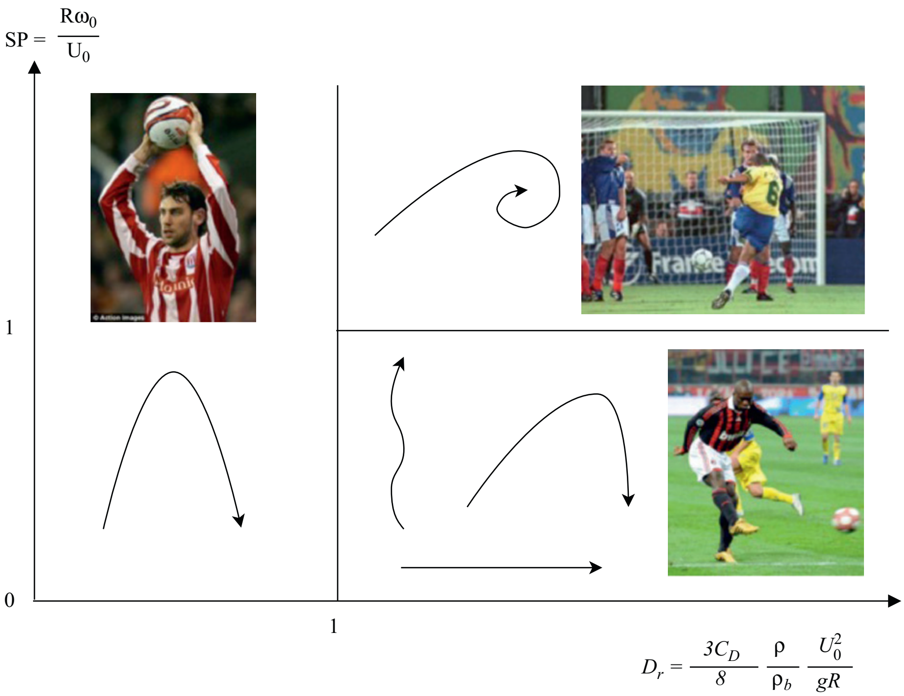

Fig. 2. Phase diagram for the different curves and associated football kicks. (Credits: Action Images, Press Association and Getty Images.)

presented in Fig. 2. We call drag number, $D_r = F_D/F_G$, the ratio between drag and weight and spin number, $S_p = F_L/F_D$, the lift to drag ratio. Using ρ for the air density, M and R for the ball mass and radius, U_0 and ω_0 for its velocity and spin, these forces can be expressed as $F_G = Mg$, $F_D = 1/2\rho C_D \pi R^2 U_0^2$ and $F_L = 2C_n \rho \pi R^3 \omega_0 U_0$. For Re $\approx 10^5$, $C_D \approx 0.4$ (see Section 4) and $C_n \approx 0.1$ (Nathan, 2008). Hence we deduce the expressions for the drag and spin numbers:

$$D_r = \frac{3C_D}{8}\frac{\rho}{\rho_b}\frac{U_0^2}{gR} \quad \text{and} \quad S_p = \frac{R\omega_0}{U_0}. \tag{1}$$

The density ρ_b which appears in D_r is the ball density. We dropped the factor $4C_n/C_D \approx 1$ in front of the spin number to keep the same expression as the one usually used (Nathan, 2008; Hong et al., 2010). In soccer, the mass and the radius of the ball are fixed, $M = 450$ g and $R = 0.11$ m and one deduces $\rho_b \approx 81$ kg/m^3. The drag number has been introduced as a ratio of forces, but it can also be seen as a ratio of velocities, $U_0/U^\star$, where $U^\star \equiv \sqrt{8\rho_b gR/3\rho C_D} \approx 20$ m/s. $U^\star$ is the characteristic speed above which aerodynamics dominates gravity. In the limit of small drag numbers, one expects the classical gravitational parabola (Section 3). For large drag numbers, several trajectories can be observed, depending on the spin number. Zigzag, straight lines and truncated parabola will appear for small S_p (Sections 4 and 5) while the spiral will dominate at large spin numbers (Section 6).

Table 1
Heavy kick table.

Player	U_0 (m/s)	Game
David Hirst	51	Sheffield/Arsenal (09/16/96)
David Beckham	44	Man Utd/Chelsea (02/22/97)
David Trezeguet	43	Monaco/Man Utd (03/19/98)
Richie Humphreys	42.8	Sheffield/Aston Villa (08/17/96)
Matt Le Tissier	39	Southampton/Newcastle (01/18/97)
Alan Shearer	38.3	Newcastle/Leicester (02/02/97)
Roberto Carlos	38.1	Brazil/France (06/03/97)

(a) (b)

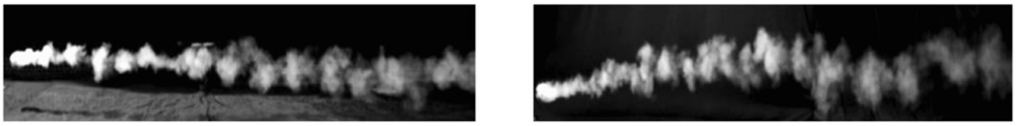

Fig. 3. Ball trajectories extracted from Hong et al. (2010): (a) straight line trajectory; (b) zigzag trajectory.

3. Parabola

In the low velocity regime $U_0 \ll U^\star \approx 20$ m/s, the ball does not feel the surrounding air and its trajectory is governed by gravity: $M\, d\underline{U}/dt = M\underline{g}$. This equation leads to the classical parabola: $y = \tan\alpha x - gx^2/2U_0^2\cos^2\alpha$. In this expression, α stands for the direction (defined from the horizontal). Such parabolic trajectories can be seen during a throw-in or a lob. The ball rises up to a maximal height $U_0^2/2g$ and then falls back at a distance $L=(U_0^2/g)\sin 2\alpha$ from its origin.

We report in Table 1 the velocities of the strongest heavy kicks. They all stand above 38 m/s which implies that the parabolae cannot be the only curve observed.

4. Straight lines and zigzags

At large velocities ($U_0 \gg U^\star$), we enter the aerodynamic domain. Without spin (spinning balls are considered in Section 6), the ball mainly experiences the drag force F_D. Typical ball trajectories obtained in this regime are presented in Fig. 3. These trajectories are extracted from the work of Hong et al. (2010): the fluid around the ball in flight is visualized using a smoke agent (titanium tetrachloride), which reveals a complex vortex dynamics. In soccer where $1\,\text{m/s} < U_0 < 50\,\text{m/s}$, the Reynolds number $\text{Re} = \rho U_0 R/\eta$ lies in the range $10^4 < \text{Re} < 5\times10^5$. The vortex shedding from spheres at large Reynolds number ($200 < \text{Re} < 3\times10^6$) has been studied by Achenbach (1974) and we report in Fig. 4 his main conclusions: the sphere wake is not axisymmetric (Fig. 4(a)) and the frequency f of vortex shedding slightly increases with the Reynolds number (Fig. 4(b)). The non-axisymmetric wake implies that a sphere placed in a uniform flow is subjected to a side force at Reynolds numbers between 200 and 10^6. The direction of the side force is random (Taneda, 1978) and for a non-spinning sphere, one expects the mean trajectory to be close to a straight line as in Fig. 3(a).

Concerning the drag coefficient C_D, Fig. 4(c) shows the classical result: as the Reynolds number is increased, C_D experiences a violent transition from a constant value 0.44 down to 0.2. The critical Reynolds number of the transition depends on the roughness of the sphere: it is 3×10^5 for a smooth sphere and 2×10^5 for a soccer ball (Asai et al., 2007). In all the present study, we do not discuss the effect of the transition on the ball trajectory and assume that its major portion is achieved in the constant $C_D \approx 0.4$ regime.

Due to the drag force, the ball velocity decreases along the trajectory. To quantify the decrease of the velocity, we consider the equation of motion: $M\, d\underline{U}/dt = -1/2\rho C_D \pi R^2 U\underline{U}$. Integrating along the trajectory of the ball (parametrized by its curvilinear coordinate) with the initial condition $U(s=0)=U_0$, we obtain:

$$U(s) = U_0 e^{-s/\mathcal{L}}, \tag{2}$$

with

$$\mathcal{L} = \frac{8\overline{\rho}}{3C_D}R \quad \text{with} \quad \overline{\rho} = \left(1 + C_M\frac{\rho}{\rho_b}\right)\frac{\rho_b}{\rho}. \tag{3}$$

$C_M \approx 1/2$ (Batchelor, 1967) stands for the added mass coefficient. The velocity thus decreases exponentially, with a characteristic penetration length $\mathcal{L}$, which is of the order of 50 m in football. The straight line will be observed if the length of the trajectory is small compared to $\mathcal{L}$.

Large sidewise deviations (several ball diameters) from this straight trajectory are, however, observed, as shown in Fig. 3(b). In baseball, such zigzagging paths are known as knuckleball effect (Watts and Sawyer, 1974). Even if this effect is

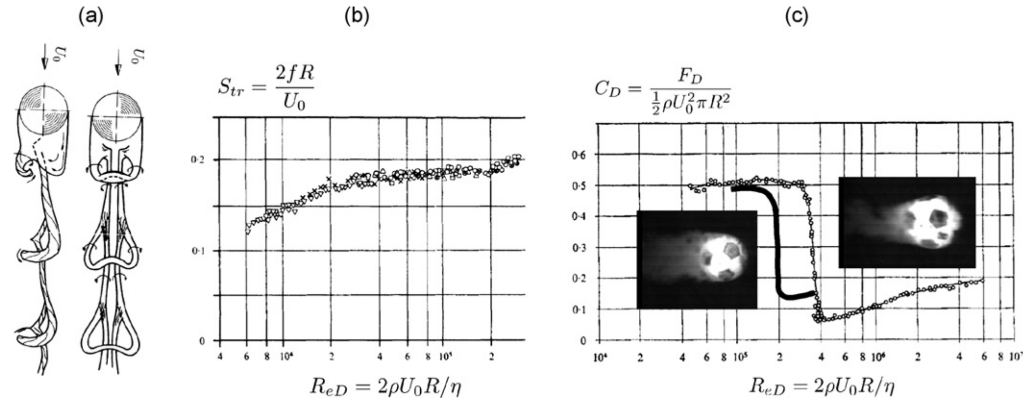

Fig. 4. Vortex structure behind a sphere extracted from Achenbach (1974): (a) schematic representation of the vortex configuration in the wake of spheres at $2\mathrm{Re}=10^3$; (b) Strouhal number vs. Reynolds number for spheres; (c) drag coefficient of the smooth sphere as a function of Reynolds number. The figure is extracted from Achenbach (1972). The solid black line and the soccer ball pictures with associated wakes are extracted from Asai et al. (2007).

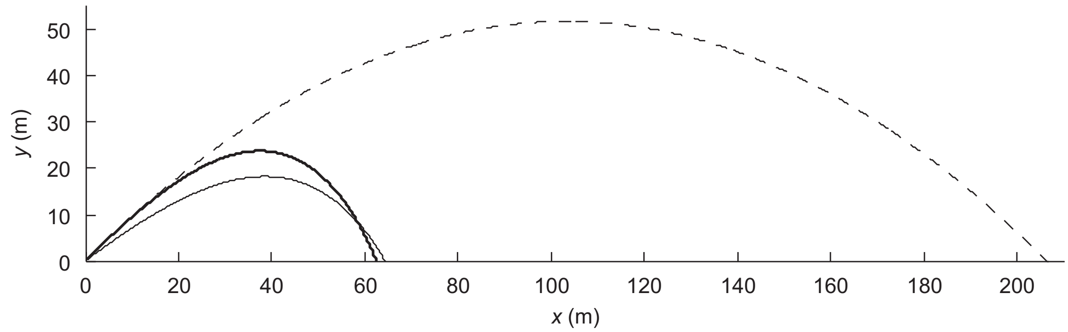

Fig. 5. Trajectories of a ball: with gravity and aerodynamic (bold solid line) and with gravity only (dashed line). The initial velocity is $U_0=45$ m/s, the initial angle is 45° and the characteristics of the ball are the ones of a soccer ball ($\overline{\rho}=74, R=11$ cm). For the third trajectory (thin solid line), only the initial angle is changed to 37°: with friction, 45° is no more the optimal angle to cover the longest length.

not yet completely quantified, the published studies associate this knuckleball effect to a low spin of the ball. According to Watts and Sawyer (1974), the seams play a crucial role in the coupling between spinning ball and the associated spinning wake. For knuckleball in soccer such as the one presented in Fig. 3(b), Hong et al. (2010) reports a spin parameter of the order of $R\omega_0/U_0 \approx 0.02$.

5. Truncated parabola

At large velocities, $U_0 \gg U^\star$, we have just shown that the trajectory is a portion of a straight line or a zigzag, when observed on a length scale smaller than $\mathcal{L}$. We discuss here the case where both gravity and aerodynamic effects influence the trajectory.

In this regime, the equation of motion is $M\, d\underline{U}/dt = M\underline{g} - 1/2\rho C_D \pi R^2 U \underline{U}$, we compute it in the case of soccer ($\mathcal{L}=54$ m). Fig. 5 shows the trajectory of the ball, compared to the theoretical parabola. We first observe that aerodynamics strongly limits the trajectory of the ball and saturates at a value close to $\mathcal{L}$. This explains why after a clearance the ball hardly passes the midfield, and always seems to come vertically on the players.

Another noticeable effect of the aerodynamic friction is the optimal angle to reach the longest distance. As shown in Fig. 5, it is smaller than 45° (around 37° in this example), the optimal angle with the parabola. Indeed, the horizontal velocity decreasing, there is a balance between going high (not to fall too quickly) without losing too much energy in the vertical motion.

6. Spiral

In the previous section, we saw how gravity can bend the trajectory once U becomes smaller than $U^\star$. Without gravity ($U \gg U^\star$), we now show that the trajectory of a spinning ball is a spiral that might be observed in some special free kicks.

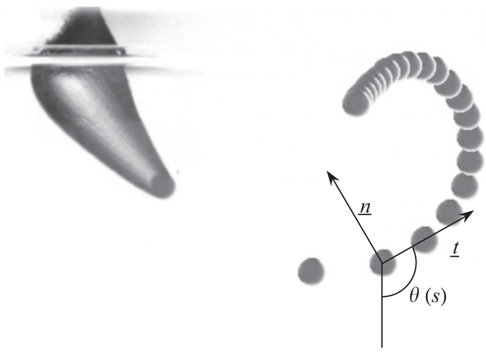

Fig. 6. Multi-pose image showing the trajectory of a spinning ball. The time step between successive ball locations is $\Delta t = 10$ ms. (Taken from Dupeux et al. (2010).)

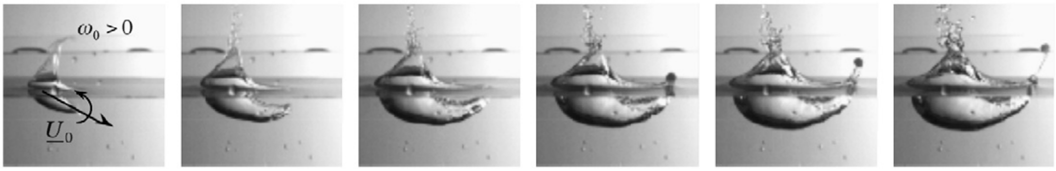

Fig. 7. Effect of the spin on the trajectory of a sphere (density ρ_b) after impact in water: U_0=20 m/s, R=2.4 mm, $\rho_b = 920$ kg/m^3,$\omega_0 = 1740$ rad/s, $\Delta t = 3.75$ ms. (Taken from Dupeux et al. (2010).)

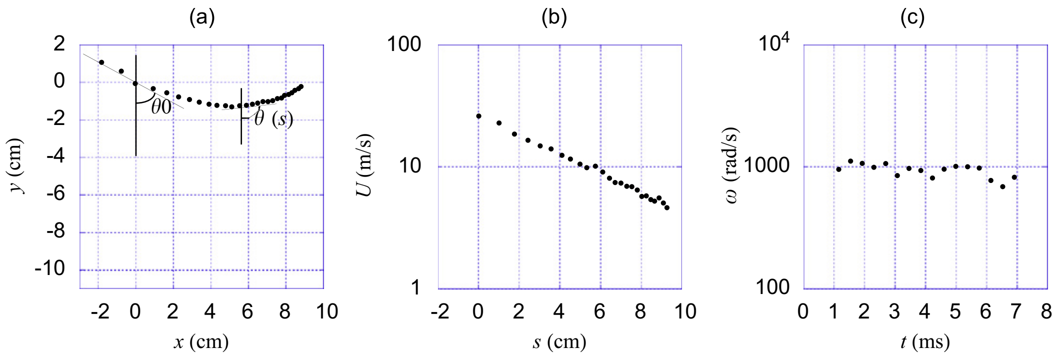

Fig. 8. (a) Trajectory of a ball (radius R=3.5 mm, density $\rho_b = 920$ kg/m^3) impacting water with a velocity U_0=27 m/s, a spin $\omega_0 = 1000$ rad/s and an inclination angle $\theta_0 = 70^\circ$. The time step between two data points is $\Delta t = 384$ μs. (b) Evolution of the corresponding velocity as a function of the curvilinear coordinate s in a semi-log plot. (c) Time variation of the corresponding rotation speed ω of the ball. (Taken from Dupeux et al. (2010).)

This spiral is presented in Fig. 6. In order to achieve this low gravity limit, we use isodensity spinning spheres in water. The detailed study of the spiral is reported in Dupeux et al. (2010) and we just recall its main properties.

6.1. Experimental facts

Qualitatively, the effect of a positive spin (anti-clockwise) is illustrated in the chronophotography in Fig. 7. The ball gets deviated from a straight line and the trajectory is bent (the ball can even come out of the bath, in Fig. 7). More quantitatively, we show in Fig. 8(a) the trajectory of a polypropylene ball ($\rho_b/\rho = 0.92$) of radius R=3.5 mm thrown in water at a velocity U_0=27 m/s, with a spin rate $\omega_0 = 1000$ rad/s, and an impact angle $\theta_0 = 70^\circ$ (defined from the vertical). In this trajectory, the constant time step between two data points is $\Delta t = 384$ μs. Clearly, the velocity of the ball decreases as it moves through water (Fig. 8(a)). The evolution of the ball velocity is reported in Fig. 8(b), as a function of the curvilinear coordinate s (s=0 at impact). The semi-log presentation stresses that the velocity decreases exponentially with s (Eq. (2)). The characteristic length for the decrease is 5.5 cm. Despite a strong variation of the velocity, the spin rate ω remains almost constant as the ball moves through water, as demonstrated in Fig. 8(c). This difference between the U- and the ω-variation is discussed in the following section, and shown to be the key fact to account for the spiral trajectory.

6.2. Model

The motion of the sphere is described in the Serret–Frenet coordinate system ($\underline{t}$,$\underline{n}$) introduced in Fig. 6. We first focus on the direction $\underline{t}$. As shown in the Section 5, the velocity of the ball decreases exponentially in water (Eq. (2)), with a characteristic penetration length $\mathcal{L} \approx 7\overline{\rho}R \approx 10R$. This behavior agrees with the results displayed in Fig. 8(b).

Along $\underline{n}$, the ball is subjected to a lift force $F_L = \rho\Gamma URC_n$ resulting from the circulation $\Gamma = 2\pi R^2\omega$. In our experiment $\mathrm{Re} \approx 10^4$ and the value of C_n is close to 0.13 (Nathan, 2008). The equation of motion leads to the curvature of the trajectory:

$$\left(\frac{d\theta}{ds}\right) = \frac{3}{2}\frac{C_n}{\overline{\rho}}\frac{\omega}{U}. \tag{4}$$

6.3. The ideal spiral

The next step in the derivation of the ball trajectory is to assume that the circulation Γ remains (almost) constant during the motion, as suggested by Fig. 8(c). The actual variation of the spin rate is studied by Dupeux et al. (2010). For $\omega \approx \omega_0$, the curvature of the trajectory scales like $d\theta/ds \sim \omega_0/U \sim \omega_0/U_0 e^{s/\mathcal{L}}$. The deviation of the ball from its initial orientation θ_0 thus increases exponentially with the curvilinear coordinate s, which defines the spinning ball ideal spiral. The characteristic length L_{spiral} for which the spiral coils up can be approximated to $\mathcal{L}\ln(1+1/S_p)$. Without spin ($S_p=0$), the spiral is not observed ($L_{spiral} \to \infty$). In the range of spin numbers we find in football ($S_p \lesssim 0.2$), the spiral is observed at a distance from the impact close to $\mathcal{L}$. We compare in Fig. 9(a) the observed trajectory (■) to Eq. (4) (solid line). The theoretical prediction is in close agreement with the experimental path up to the point where the ball escapes from the bath, whose surface is defined by $y=0$.

6.4. Shots in soccer

The structure of drag and lift forces obtained in water is similar to the ones obtained in air (Dupeux et al., 2010). The above model can thus be used to study the trajectory of any sphere moving with a spin in a fluid, either liquid or gas. In soccer, the characteristic length of the spiral $\mathcal{L}$ is smaller than the size of the field. Provided that the shot is strong enough to neglect gravity ($U_0 \gg U^\star$) and long enough ($\sim \mathcal{L}$), a highly curved trajectory can be observed. We can define three kinds of shots, depending on the distance to the goal: the penalty (9 m), the close free kick ($\sim$ 20 m) and the distant free kick ($\sim$ 35 m). Since $\mathcal{L}$ is independent of the velocity U_0 and of the rotation ω_0 of the ball, the trajectories are quite different, as shown in Fig. 10. For the penalty, the ball follows the very beginning of the spiral, i.e. a straight line, whereas in the close free kick the

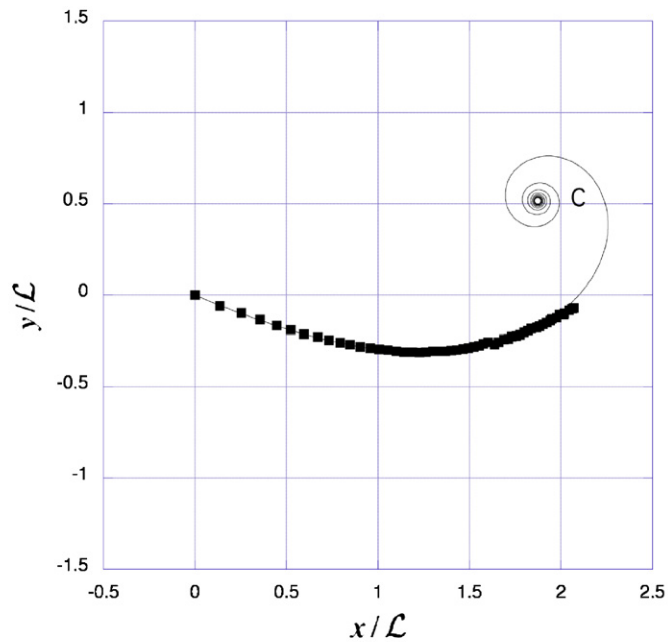

Fig. 9. Characteristics of the ideal spiral spinning ball: the trajectory of the ball is plotted in the plane ($x/\mathcal{L}$,$y/\mathcal{L}$) for U_0=32 m/s, R=3.6 mm, $\theta_0 = 67^\circ$, $\omega_0 = 743$ rad/s and $\rho_b/\rho = 1.4$. The experimental data are presented with the ■ symbol while the theoretical shape (Eq. (4)) is drawn with a solid thin line (y=0 is the surface of the water bath). (Taken from Dupeux et al. (2010).)

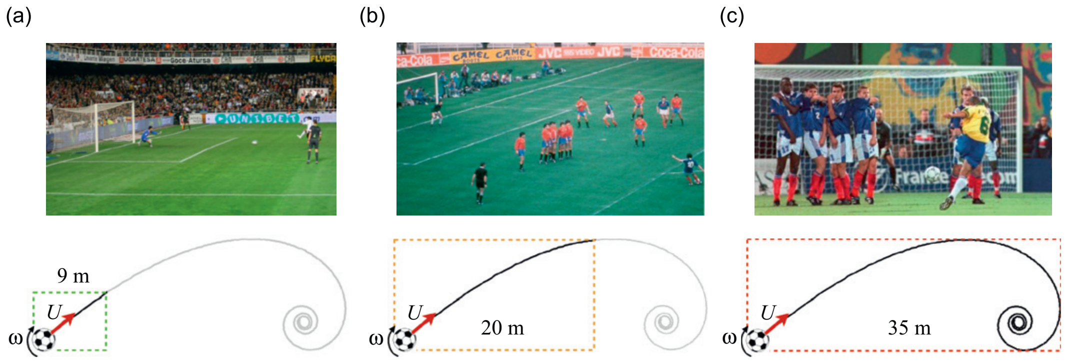

Fig. 10. Three kind of shot in soccer: (a) penalty, (b) close free kick, (c) distant free kick. (Credits: (a) Michael Bryan, (b) Panoramic, (c) Press Association.)

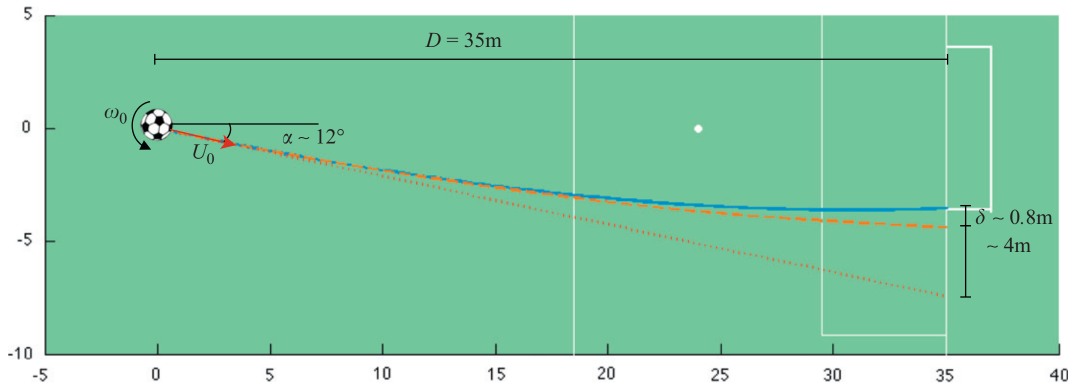

Fig. 11. The goal of Roberto Carlos against France in 1997. The blue plain line is the real trajectory of the ball, calculated from Eq. (4) with $U_0 = 38$ m/s and $\omega_0 = 88$ rad/s. The orange dashed line shows the circle trajectory and the doted red line a straight one. (For interpretation of the references to color in this figure legend, the reader is referred to the web version of this article.)

trajectory is close to a circle: this is the curve we generally see most of the time with a spinning ball. For the distant free kick, the distance to the goal is comparable to $\mathcal{L}$, so that we expect not a circle but a spiral trajectory.

This is the way we interpret a famous goal by the Brazilian player Roberto Carlos against France in 1997 (http://www.youtube.com/watch?v=crSkWaJqx-Y). This free kick was shot from a distance of 35 m. Roberto Carlos strongly hits the ball ($U_0 = 38$ m/s) with an angle of about 12° relative to the direction of the goal; due to the rotation ($\omega_0 \approx 88$ rad/s, a value difficult to extract from the movies, yet plausible), it sidestepped the wall, bent toward the goal, hit the goal post and entered (Fig. 11). The goalkeeper Fabien Barthez did not move: without rotation, the ball would have left the field 4 m away from the goal! If the trajectory had been simple circle and not a spiral, the ball would have been still 1 m away, as shown below.

We can estimate the distance δ between the circle and the spiral trajectory on the goal line (as defined in Fig. 11). Using Eqs. (2) and (4), we find $\delta \approx D^3/6R_0\mathcal{L}\cos^2\alpha$ where D is the distance to the goal, α is the initial angle and R_0 is the initial curvature of the trajectory (given by Eq. (4) for $\omega = \omega_0$ and $U = U_0$). If we compare δ to the size R of the ball, we get $\delta/R \sim (D/D^*)^3$ where $D^* \equiv (\mathcal{L}R_0R)^{1/3}$ is the distance over which the trajectory differs by a distance R from the circle. Beyond D^* ($D^* \approx 10$ m for Roberto Carlos's free kick), δ increases rapidly: for $D = 35$ m, δ it becomes nearly 1 m, a distance large enough to surprise a goalkeeper.

7. Physical classification of sports

We have discussed so far the different trajectories that can be observed in soccer. We now try to extend this study to other sports. For each sport, Table 2 presents the ball size, the density ratio, the maximum ball velocity, the characteristic spin parameter and the size of the field, L_{field}. In the special case of baseball, L_{field} represents the distance between the pitcher and the batter. Using these data, we display the penetration length $\mathcal{L} = 7\overline{\rho}R$ and the length scale U_0^2/g on which gravity acts. By comparing $\mathcal{L}$ and U_0^2/g, one identifies sports dominated by aerodynamics (table tennis, golf, tennis) and sports dominated by gravity (basketball, handball). In between, we find sports where both gravity and aerodynamics play a comparable role (soccer, volleyball, baseball). Indeed, in the first category of sports, the spin is systematically used, while it is not relevant in the second category; it only appears occasionally in the third one, in order to produce surprising trajectories.

Table 2
Specifications for different sports. The first three sports are dominated by aerodynamic effects ($\mathcal{L} \ll U_0^2/g$). For the last two sports, gravity dominates aerodynamics ($\mathcal{L} \gg U_0^2/g$). In between, we identify sports for which both gravity and aerodynamics can be used to control the ball trajectory. In this table, L_{field} is the size of the field except for baseball where it stands for the distance between the pitcher and the batter.

sport	$2R$ (cm)	ρ_b/ρ	U_0 (m/s)	$S=\frac{R\omega_0}{U_0}$	L_{field} (m)	$\mathcal{L}$ (m)	U_0^2/g(m)	d (m)
Table tennis	4.0	67	50	0.36	2.7	9.3	255	1
Golf	4.2	967	90	0.09	200	141	826	7
Tennis	6.5	330	70	0.19	24	73	499	5
Soccer	21	74	30	0.21	100	54	92	7
Baseball	7.0	654	40	0.17	18	160	163	7
Volleyball	21	49	20	0.21	18	35	41	5
Basketball	24	72	10		28	60	10	
Handball	19	108	20		40	71	40	

Focusing on sports where aerodynamics plays a role, we observe that the penetration length, which is also the characteristic length of the spiral, is always larger than the size of the field, except for soccer where it is 23% smaller. Since the spin parameter is smaller than one, the spiral center (Section 6.3) will lie outside the field. This suggests that the ball trajectory (4) can be expanded for $s/\mathcal{L} \ll 1$. In this limit, the spiral reduces to a circle and we can evaluate the length d by which the ball deviated from its initial direction by its own size R: $d \approx \sqrt{2\mathcal{L}R/\Delta S}$. This distance is shown in the last column of Table 2. It is found to be systematically smaller than L_{field}, the field size, which makes relevant to the use of spin effects to control the trajectory of the ball.

8. Conclusions

The trajectory of a soccer ball is dictated by three different forces, gravity, drag and lift. We propose a phase diagram to classify the different trajectories according to the relative magnitude of these three forces. When gravity dominates, the classical parabola is expected. When aerodynamics dominates, one expects a straight trajectory without spin. This is almost true apart from the floating ball regime which leads to zigzag motions. Even if this regime is clearly related to the emission of vortical structures, its precise description still need to be done. For very long shots, gravity cannot be neglected and the ball follows a truncated parabola. Finally, in the case of spinning balls, aerodynamics imposes a spiral trajectory. The comparison between the characteristic size of the spiral and of the parabola makes it possible to classify the different ball sports in three categories, the ones dominated by gravity, the ones dominated by aerodynamics and the ones where both effects can be used.

References

Achenbach, E., 1972. Experiments on the flow past spheres at very high Reynolds numbers. Journal of Fluid Mechanics 54, 565–575.
Achenbach, E., 1974. Vortex shedding from spheres. Journal of Fluid Mechanics 62, 209–221.
Asai, T., Carre, M.J., Akatsuka, T., Haake, S.J., 2002. The curve kick of a football I: impact with the foot. Sports Engineering 5, 183–192.
Asai, T., Seo, K., Kobayashi, O., Sakashita, R., 2007. Fundamental aerodynamics of the soccer ball. Sports Engineering 10, 101–110.
Batchelor, G.K., 1967. An Introduction to Fluid Dynamics. Cambridge University Press.
Blanchard, K., 2005. The Anthropology of Sport. Bergin & Garvey (ISBN 0897893298).
Bull Andersen, T., Dörge, H.C., Thompsen, F.I., 1999. Collision in soccer kicking. Sports Engineering 3, 121–125.
Carre, M.J., Asai, T., Akatsuka, T., Haake, S.J., 2002. The curve kick of a football II: flight through the air. Sports Engineering 5, 193–200.
Craig, S., 1961. Sports and games of the ancients (ISBN 0313361207).
Dupeux, G., Le Goff, A., Quéré, D., Clanet, C., 2010. The spinning ball spiral. New Journal of Physics 12 (9), 093004.
Greenhough, J., Birch, P.C., Chapman, S.C., Rowlands, G., 2002. Football goal distributions and extremal statistics. Physica A 316, 615–624.
Guttmann, A., Thompson, L.A., 2001. Japanese sports: a history. University of Hawaii Press (ISBN 0824824644).
Haddadin, S., Laue, T., Frese, U., Wolf, S., Schaffer, A.A., Hirzinger, Z., 2009. Kick it with elasticity: safety and performance in humanrobot soccer. Robotics and Autonomous Systems 57, 761–775.
Hill, W.D., Blake, M., Clark, J.E., 1998. Ball court design dates back 3,400 years. Nature 392, 878.
Hong, S., Chung, C., Nakayama, M., Asai, T., 2010. Unsteady aerodynamic force on a knuckleball in soccer. Procedia Engineering 2, 2455–2460.
Hosler, D., Burkett, S., Tarkanian, M., 1988. Prehistoric polymers: rubber processing in ancient Mesoamerica. Science 284, 5422.
Ishii, H., Yanagiya, T., Naito, H., Katamoto, S., Maruyama, T., 2009. Numerical study of ball behavior in side-foot soccer kick based on impact dynamic theory. Journal of Biomechanics 42, 2712–2720.
Larson, O., 2001. Charles Reep: a major influence on British and Norwegian Football. Soccer & Society 2, 58–78.
Malacarne, L.C., Mendes, R.S., 2000. Regularities in football goal distributions. Physica A 286, 391–395.
Mehta, R.D., 1985. Aerodynamics of sports balls. Annual Review of Fluid Mechanics 17, 151–189.
Mendes, R.S., Malacarne, L.C., Anteneodo, C., 2007. Statistics of football dynamics. European Physical Journal B 57, 357–363.
Miller, S.G., 2006. Ancient Greek Athletics. Yale University Press.
Murray, B., 1998. The world's game: a history of soccer (ISBN 0-252-06718-5).
Nathan, A.M., 2008. The effect of spin on the flight of a baseball. American Journal of Physics 76, 119–124.
Reep, C., Benjamin, B., 1968. Skill and chance in Association Football. Journal of the Royal Statistical Society. Series A (General) 131, 581–585.
Reep, C., Pollard, R., Benjamin, R., 1971. Skill and chance in ball games. Journal of the Royal Statistical Society. Series A (General) 134, 623–629.

Ribeiro, H.V., Mendes, R.S., Malacarne, L.C., Picoli, S., Santoro, P.A., 2010. Dynamics of tournaments: the soccer case. A random walk approach modeling soccer leagues. European Physical Journal B 75, 327–334.
Taneda, S., 1978. Visual observations of the flow past a sphere at Reynolds numbers between 10^4 and 10^6. Journal of Fluid Mechanics 85, 187–192.
Watts, R.G., Sawyer, E., 1974. Aerodynamics of a knuckleball. American Journal of Physics 43, 960–963.